Real time Measurement of Dynamic Wheel-Rail Contacts Using Ultrasonic Reflectometry

Lu Zhou[1], Henry Brunskill[1], Martin Pletz[2], Werner Daves[2,3], Stephan Scheriau[4], Roger Lewis[1]*.

[1] Department of Mechanical Engineering, The University of Sheffield, Mappin Street, S1 3JD, Sheffield, United Kingdom
[2] Department of Polymer Engineering and Science, Montanuniversitaet Leoben, Austria
[3] Institute of Mechanics, Montanuniversitaet Leoben, Leoben, Austria
[4] voestalpine Schienen GmbH, Leoben, Austria
*corresponding author: roger.lewis@sheffield.ac.uk

Abstract

The contact condition between the wheel and the rail is paramount to the lifespan, safety and smooth operation of any rail network. The wheel/rail contact condition has been estimated, calculated and simulated successfully for years, but accurate dynamic measurement has still not been achieved. Methods using pressure sensitive films and controlled air flow have been employed, but are both limited.
The work described in this paper has enabled, for the first time, the measurement of a dynamic wheel/rail contact patch using an array of 64 ultrasonic elements mounted in the rail. Previous work has successfully proved the effectiveness of ultrasonic reflectometry for static wheel/rail contact determination. The dynamic real-time measurement is based on previous work, but now each element of an array is individually pulsed in sequence to build-up a linear measurement of the interface. These cross-sectional, line measurements are then processed and collated resulting in a 2-dimensional contact patch. This approach is able to provide not only a contact patch, but more importantly, a detailed and relatively high-resolution pressure distribution plot of the contact. FE predictions have also been carried out for validation. Work is now underway to increase the speed of the measurement.

Keywords: wheel/rail contact, measurement, real-time, contact pressure.

1 Introduction

Contact conditions are vital to the life prediction, daily maintenance, profile design and safety of rail tracks. Research and investigations have been undertaken for years to study the wheel/rail contact. Due to the complexity of the dynamic wheel/rail interface, no practical methods can truly reflect conditions near the contact area. Although controlled air flow [1] and pressure sensitive films [2] have been developed for contact characterization, these are respectively limited by resolution and because the technique affects the contact. Numerical methods have been proposed [3, 4] for wheel/rail contact prediction following Kalker's work [5, 6]. With the development of computing software, finite element methods (FEM) have been more and more utilized to simulate static and dynamic wheel/rail contacts in various conditions [7, 8]. However, the difficulties in simulating real surfaces with surface roughness and wear evolution put forward doubts as to whether FEM results are accurate. Numerical

methods and particularly, FEMs need good validation from an effective experimental approach.

Ultrasound reflectometry being a non-destructive measuring technique, has been successfully applied on a variety of static machine-element contacts including bolted joints, ball bearings, press fits [9] as well as wheel and rail specimens [10, 11, 12]. The technique involves pulsing an ultrasonic pressure wave towards the contact interface and deriving information from reflected signals. For a perfectly bonded contact pair, the proportion of reflected signal, known as reflection coefficient *R*, is dependent on the acoustic impedance *z*, of the materials and is determined by the following relationship:

$$R = \frac{z_1 - z_2}{z_1 + z_2} \tag{1}$$

where z_1 and z_2 are the acoustic impedances of material 1 and 2 respectively (a multiplication of density and speed of sound in the material). Hence the acoustic impedance of air is far smaller than that of a solid. As the ultrasonic wave reaches the solid-air interface, almost all of it will be reflected. Through this, it is possible to characterise a contact using ultrasonic reflectometry.

For machine-elements no surface is smooth, asperities are present and roughness inherently exists. When two solids are pressed together, it is those asperities that are actually in contact with each other and thus air gaps are formed in between them at the interface. The ultrasonic wave incident at the interface is transmitted at points of contact and is reflected at the air gaps. The behaviour of asperities is modelled with a quasi-static spring approach [13]. As the load is increased, the asperities deform more and are further pressed together, resulting in a greater amount of ultrasonic signal transmission due to an increase in the interfacial stiffness as analogized as springs under deformation, as shown in Figure 1.

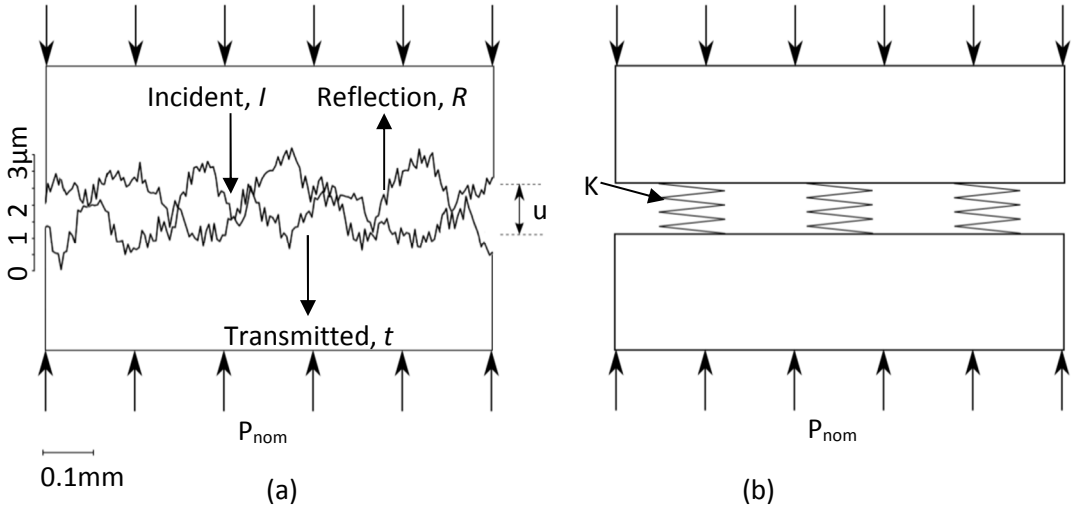

Figure 1: (a) a diagram showing to scale the surface asperities coming into contact and (b) how the interface behaves as a series of springs of stiffness *K*.

The reflection coefficient is not only dependent on acoustic impedance, but also on the stiffness and properties of the ultrasonic waves. The full form of the reflection coefficient equation is given by:

$$R = \frac{z_1 - z_2 + i\omega(z_1 z_2/K)}{z_1 + z_2 + i\omega(z_1 z_2/K)} \quad (2)$$

where $\omega = 2\pi f$ is the angular frequency of the ultrasound wave, K is the stiffness of the interface. For the case of the same or similar materials being in contact, $z_1 = z_2$ and Equation (2) can be rearranged into Equation (3), where $|R|$ is the modulus of the reflection coefficient and K can be calculated. K can be related to contact pressure with a series of calibration tests. This is carried out using two specimens of the same material and surface roughness of the test components. By applying a known load to a known contact, for instance with a flat-on-flat contact, a relationship between contact pressure and interfacial stiffness can be plotted:

$$K = \frac{\omega z}{2}\sqrt{\left(\frac{1}{|R|^2} - 1\right)} \quad (3)$$

Static wheel/rail contact patch characterisation has been carried out using a focusing transducer and a 2-dimensional map has been achieved by moving the transducer in two directions of the scanning plane step-by-step [10]. This is limited only to static tests, although it results in a high-resolution image.

Pilot studies have been carried out on quasi-static wheel/rail contact using an ultrasonic array. The wheel specimen was manually moved over the rail in which the array was mounted and measurements were taken [11, 14]. The array consists of 64 elements and each element is pulsed individually, all the elements are arranged in a line. As one contact body moves over the other, the ultrasonic signals are partially transmitted (as with the static technique) resulting in a drop of received reflected signals. The resulting cross-sectional line measurements are then processed and translated into a 2-dimensional contact patch map. In this paper the technique was advanced to fully dynamic measurements on a full-scale wheel/rail contact rig. Finite element analysis was also carried out as a validation.

2 Ultrasonic Measurements

2.1 Full-Scale Wheel/Rail Rig

The full-scale wheel-rail test rig (see Figure 2) used to carry out the tests is hydraulically driven and can apply a vertical load up to 200 kN. This rig has recently been re-commissioned. Previous work using the rig has involved friction and wear studies [15]. A wheel (5) is suspended on an axle which rotates in two journal bearings located in a loading frame (2) and can rotate freely. The vertical actuator (1) is used to simulate axle loads acting on the wheel. A rail section (6) is fitted and clamped at the bottom into a sliding bed with an inclination of 1 in 20. The rail is driven by hydraulic actuators (3) and can be pulled and pushed longitudinally, the wheel rotates due to friction as the rail moves.

Figure 2: Full scale wheel/rail test-rig (1: vertical actuator; 2: loading frame; 3: longitudinal drive system; 4: lateral ram; 5: wheel; 6: rail)

2.2 Test Conditions

The wheel has a worn P8 profile at a diameter of 920 mm. A 1200 mm long UIC60A rail section is used. As described in Section 2.1, the wheel rolls over the rail as the rail is pulled. During one pass the wheel rotates about 1/3 of a full revolution. For the experiments carried out here, a 200 mm long rolling path was used as the test zone. During the testing period, the wheel is lowered onto the rail by a vertical ram and loaded up, the rail is pulled forward in a longitudinal direction so that the wheel is able to roll over the rail in the opposite direction due to friction. After one pass, the rail is pushed backwards and the wheel rolls in the reverse direction. In this way two measurements are taken, one in each direction, during a full test-cycle. Since there is no constraint mechanism for wheel lateral movement, the contact position between wheel and rail is not fixed, there is a 2 mm-3 mm lateral displacement throughout one pass. Therefore, the initial contact is a tread contact, but can extend to be near the flange area at the end of the test.

2.3 Ultrasonic Equipment

A 64-element ultrasonic scanning array was used for taking measurements. The ultrasonic pulsar-receiver and data acquisition system is a FMS100 type ultrasonic computer manufactured by Tribosonics Ltd., and has 8 channels which can emit and receive ultrasonic signals simultaneously and each channel is responsible for pulsing 8 elements. The elements are arranged in a line, as shown in Figure 3. The array is 42 mm long and the actual pulsing length is 40mm.

Figure 3: Ultrasonic scanning array and multiplexor

A hole was machined on the test rail specimen to fit the array into. A holder was designed and manufactured to clamp the array in position while taking measurements. The hole is located about 1/3 of the way along length from the start of the test cycle in the longitudinal direction, as shown in Figure 4.

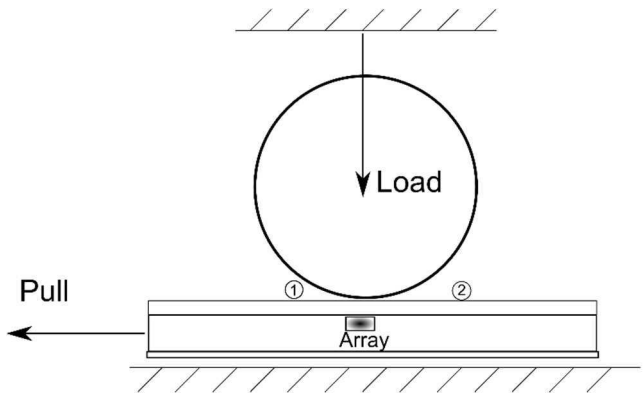

Figure 4: Array longitudinal position in the rail

In terms of lateral position, since the array is smaller than the width of the rail head, it is impossible for the scanning area to cover the whole rail head. But with proper fitting, the array is enough to capture all the contact information, as shown in Figure 5. For universal notation purposes and to avoid confusion, in this paper, the x axis always refers to the lateral direction of the rail and the y axis refers to the longitudinal (rolling) direction.

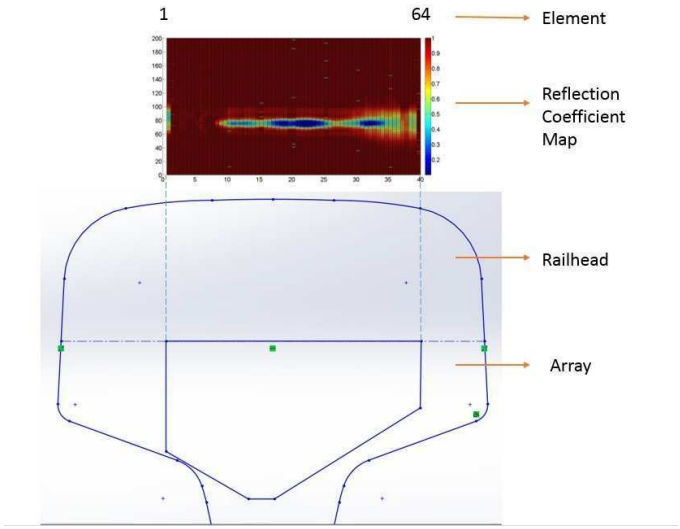

Figure 5: Array lateral position in the rail head

The array was fitted in such a way that ultrasonic signals were perpendicular to the contact region so as to get the best reflection information. When taking measurements, the elements pulse ultrasonic signals towards the rail head, which then bounce back, and the reflected signals are received by the array and processed. A limitation of the array is that only one channel (8 elements) can pulse simultaneously at any one time, therefore a multiplexor is needed to switch channels. The switching cycle is shown in Figure 6. As the array is fixed at one point in the rail and the wheel moves continually during the testing period, the multiplexor switching speed has to be fast enough so that the longitudinal offset from the measurements between channels in one switching cycle can be ignored. In that way, the array can be regarded as 64 elements pulsing and taking measurements at the same time.

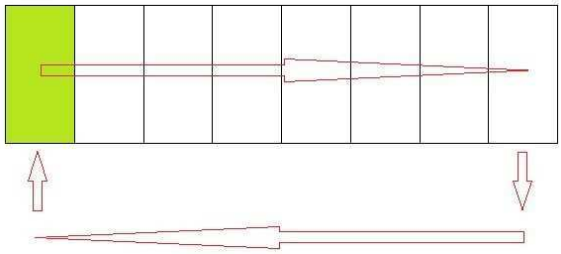

Figure 6: Switching cycle

2.4 Data Acquisition & Post-Processing

Once the full-scale rig and the scanning array has been set-up, a measurement can be carried out. The ultrasound incident signals and reflected signals are displayed in a group of 8 (one channel) on the oscilloscope with respect to time latency. The

reflected signals from the contact region are zoomed-in on and highlighted, the peak-to-peak value of each signal was recorded continually as the test proceeded (Figure 7).

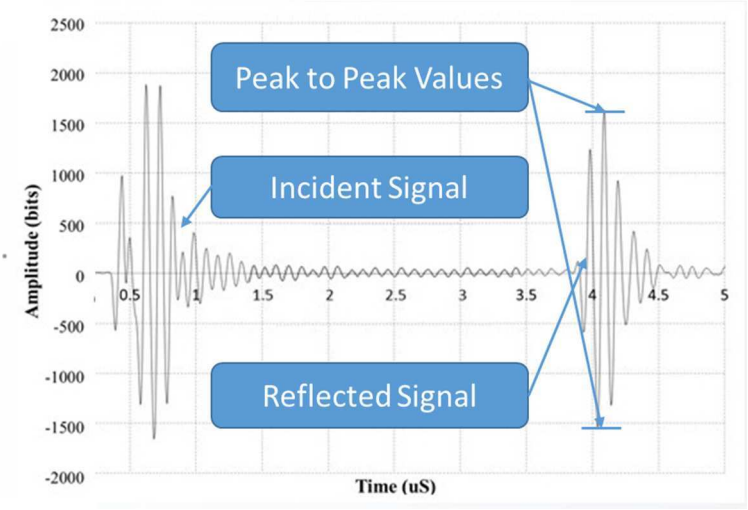

Figure 7: Ultrasound signals on oscilloscope

Each channel can pulse and take measurements twice during one switching cycle. Recorded data for each channel is then averaged and arranged in a way synchronised to match the physical arrangement of transducers in the array. After that, a row of data which has been measured outside the contact region is chosen as a reference, reflection coefficients can then be acquired by dividing all the data with corresponding reference, a map of reflection coefficients is then plotted as shown in Figure 8 (the x and y axes have been rescaled to distance.

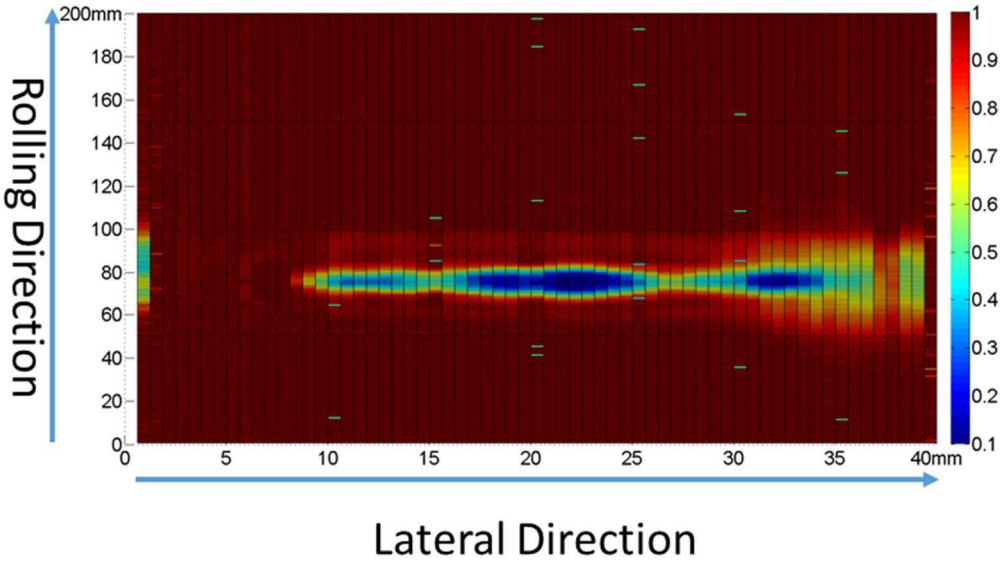

Figure 8: Reflection coefficient map of one scan

As mentioned in Section 1, for two bodies of similar or the same materials in contact against each other, the contact stiffness K can be determined by Equation (3), $|R|$ can be obtained by dividing the amplitude of reflected signals by that of incident signals.

A series of calibration tests were carried out by Marshall et al. [4] with different pairs of wheel and rail surface roughness: unused, worn tread, worn flange and sand

damaged. A calibration curve was plotted and a linear relationship between contact stiffness and contact pressure was obtained for each case respectively. For the worn tread case that applies here, the relationship between contact pressure p is:

$$p = 123K \tag{4}$$

Contact pressure maps can thus be plotted as in Figure 9. The x axis and y axis refer to 64 elements and time respectively. The resolution of the x axis is limited to the physical arrangement of the elements and so is fixed at 64. The resolution of the y axis is related to the switching speed of the multiplexor and rolling speed of the wheel, the higher the switching speed or the lower the rolling speed is, the better the resolution that can be achieved. The switching speed in tests here was 10 Hz.

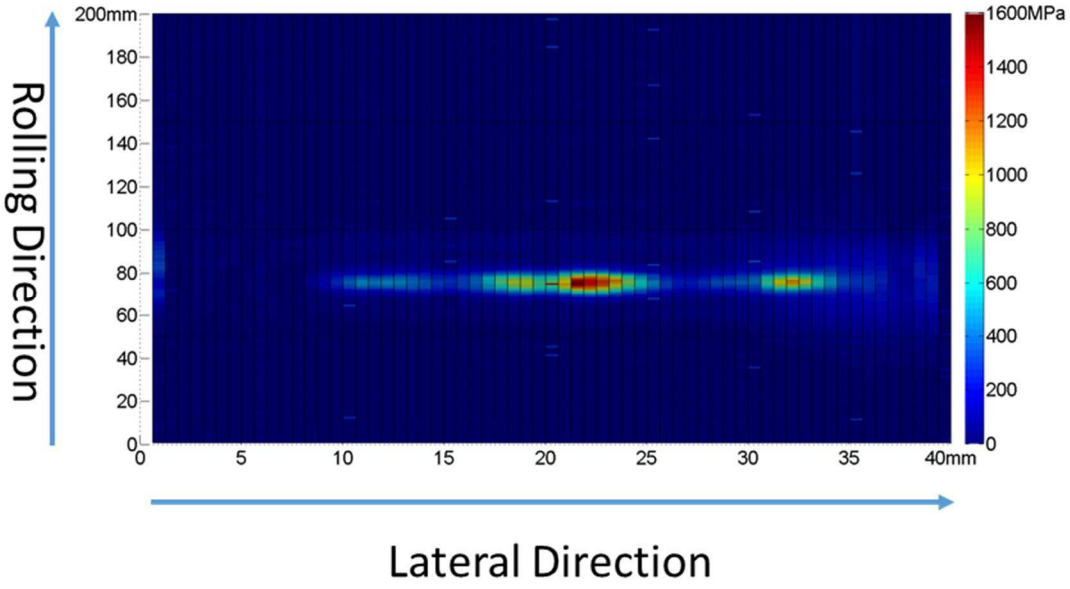

Figure 9: Contact pressure map of one scan

It should be noted that although the array is kept still measuring one area of rail head, the whole test can be regarded as the array swiping over the entire test length with the wheel rolling over a static rail at the point where the array is actually located. Therefore, the x and y axis in the contact pressure map can be translated to an actual longitudinal and lateral test length. Hence the contact pressure distribution can be displayed in a more straightforward way.

2.5 Results & Discussion

A series of measurements were taken under different loads and rolling speeds. The tests started with a load of 40 kN at a rolling speed of 1 mm/s, and then the load was increased 20 kN steps up to 120 kN (mass of the wheel was taken into account). Figure 10 shows a pair of full scans at 40 kN and 1 mm/s, the contact can be seen 1/3 of the way along the test length as would be expected. The maximum contact pressure is 678 MPa and 739 MPa respectively, and for all the loads, maximum contact pressure taken from forward and backward tests differ no more than 10%, and is found to be of the order of 5%.

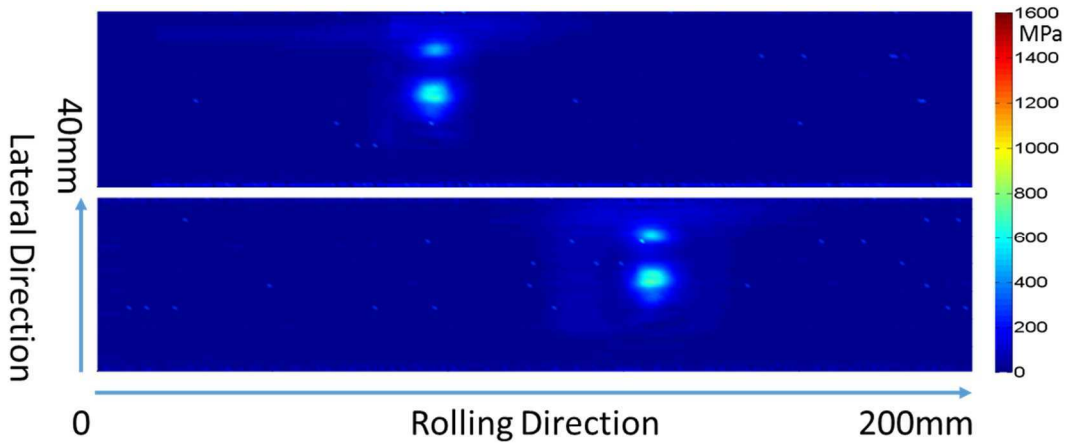

Figure 10: Full contact pressure maps at a 40 kN load at 1 mm/s

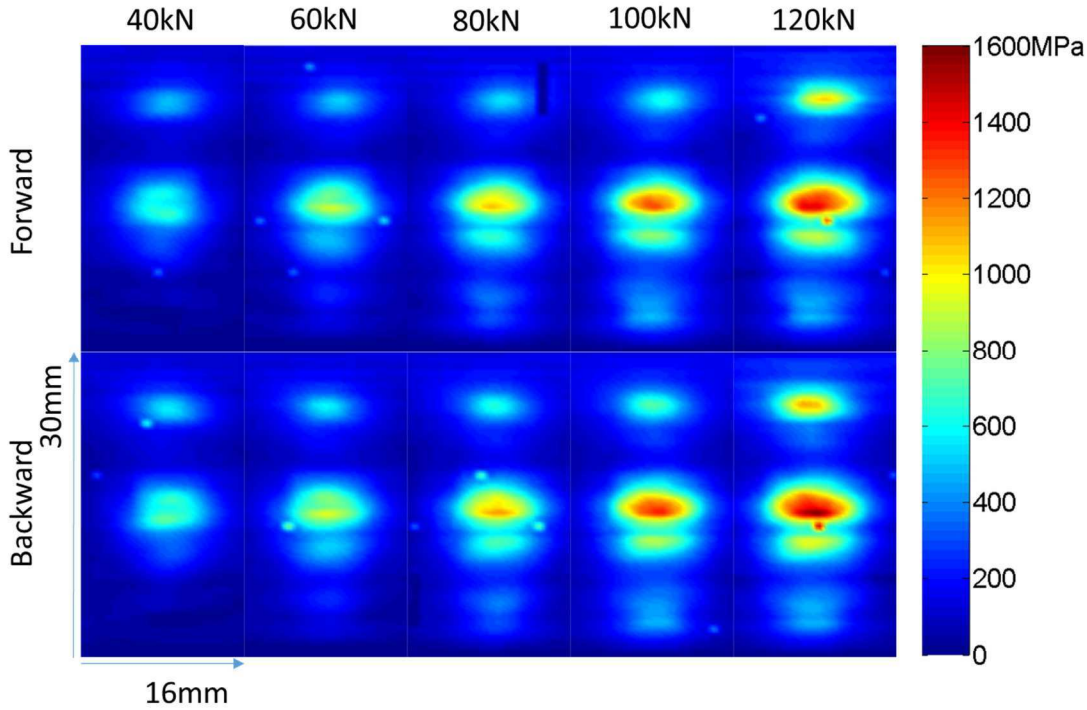

Figure 11: Contact pressure maps at 1 mm/s

Figure 11 show a series of contacts under the speed of 1 mm/s with increasing loads applied. The contacts are cut from whole scan shown in Figure 10 and interpolated for better visual effects. From the results it can be seen that contact area as well as contact pressure grows with increasing load. The contact patch grows from one side to the other and the main contact area splits into two as the load increases.

Results from the same load, but inverse rolling direction match with each other very well in terms of contact area as well as pressure distribution. This indicates that the array is capable of producing consistent, repeatable measurements.

Tests at a rolling speed of 5 mm/s were carried out with the same loads applied. The array was moved approximately 3 mm in the lateral direction compared with the first tests due to the changing contact position.

Figure 12 show a series of contacts at a speed of 5 mm/s with increasing loads applied. Compared with pressure maps of 1 mm/s tests, more "defective" cells are observed in the 5 mm/s results. This is because less information was recorded in the same time as the rolling speed increased, which led to insufficient data for averaging. However, results from 5 mm/s still have enough information for each contact generally: contact patches are nearly identical as the corresponding ones in 1 mm/s tests; contact pressure distributions also match quite well. Maximum contact pressure and contact area are plotted against load for tests at the two speeds, as shown in Figure 14. Since the difference between results from forward and backward tests is acceptable, only data from the forward tests is plotted.

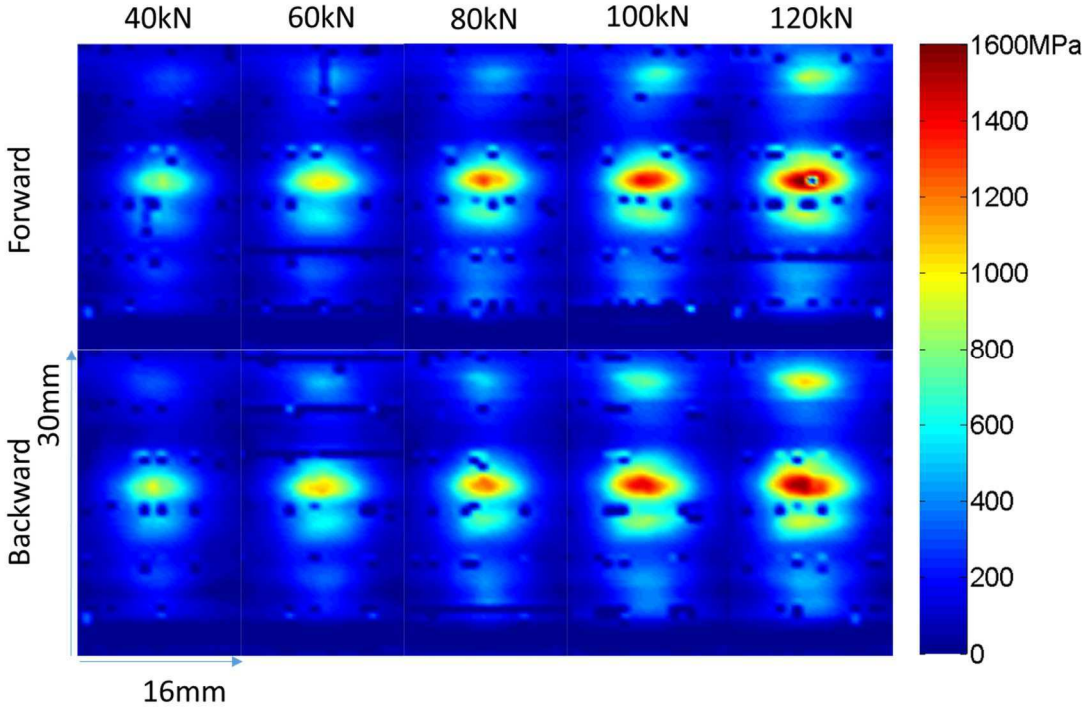

Figure 12: Contact pressure maps at 5 mm/s

In a 2-dimensional plot, the "visible" contact patches (for example as shown in Figure 12) are larger than the actual nominal contact areas. This is because the ultrasonic array is working by taking averages of all data in the region it is interrogating, and this region cannot be infinitely small, the boundary between the contact area and non-contact area is not a clear line, but a transmission area, which is noted as the "blurring" effect; Another reason is that some of the elements are scanning around areas close to the rail sides where the profile are much more curved. As the load increases, the rail will deform, any tiny deformation around the rail sides will result a large amplitude drop of reflected signals, and this effect is also captured in the 2-D plots. To determine the area, a decision must be taken on where, in terms of contact pressure, to filter out data around the contact zone. As shown in Figure 14, for wheel-rail contact

under all loads, the contact area drops continuously with the lower bound pressure going up. The contact pressure is calculated from the reflected coefficient, therefore to choose a proper bottom pressure limit, a confidence interval of reflection coefficients must be decided to distinguish contact area and non-contact area. From equation (3) and equation (4), the bottom pressure limit P_{btm} is calculated as:

$$P_{btm} = 123 \times \frac{\omega z}{2} \sqrt{\frac{1}{|R_{top}|^2} - 1} \tag{5}$$

Figure 13 shows the distribution of reflection coefficients in a lateral direction under 40 kN load. As a contact patch measured from the ultrasonic approach is normally larger than actual nominal region of contact, a cut-off reflection coefficient is necessary to for contact area calculation. With a set of validation experiments carried out by applying casting blue paint to the test wheel, and comparing ultrasonic measurements with the paint pressed on the rail head after the test, the cut-off reflection coefficient R_{top} can be selected as 0.9, through equation (5) P_{btm} is determined as 77.62 MPa, from Figure 14 the contact area under each load is 285, 354, 389, 415, 418 mm^2 for a rolling speed of 1 mm/s.

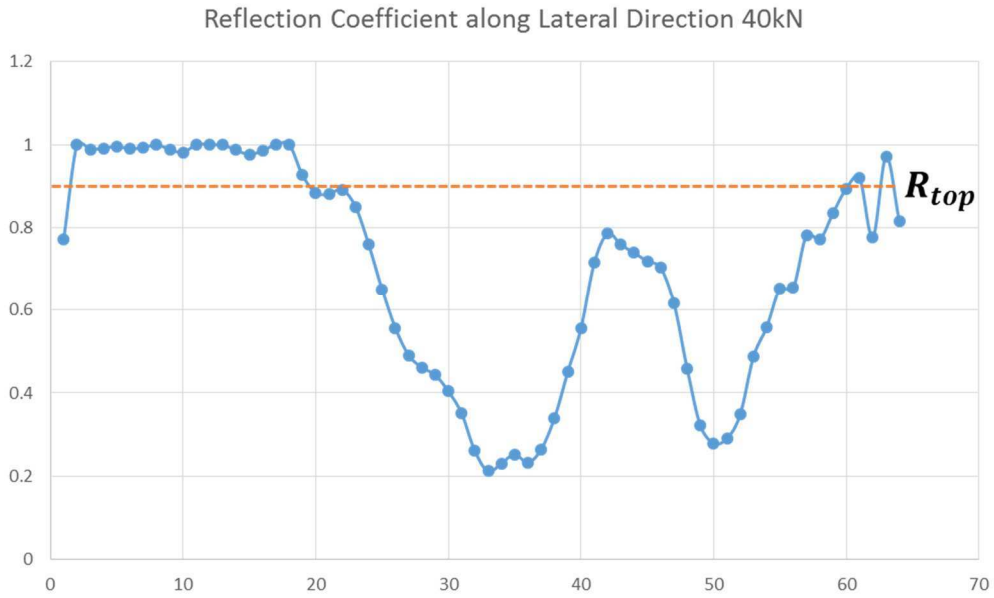

Figure 13. Reflection coefficients along lateral direction

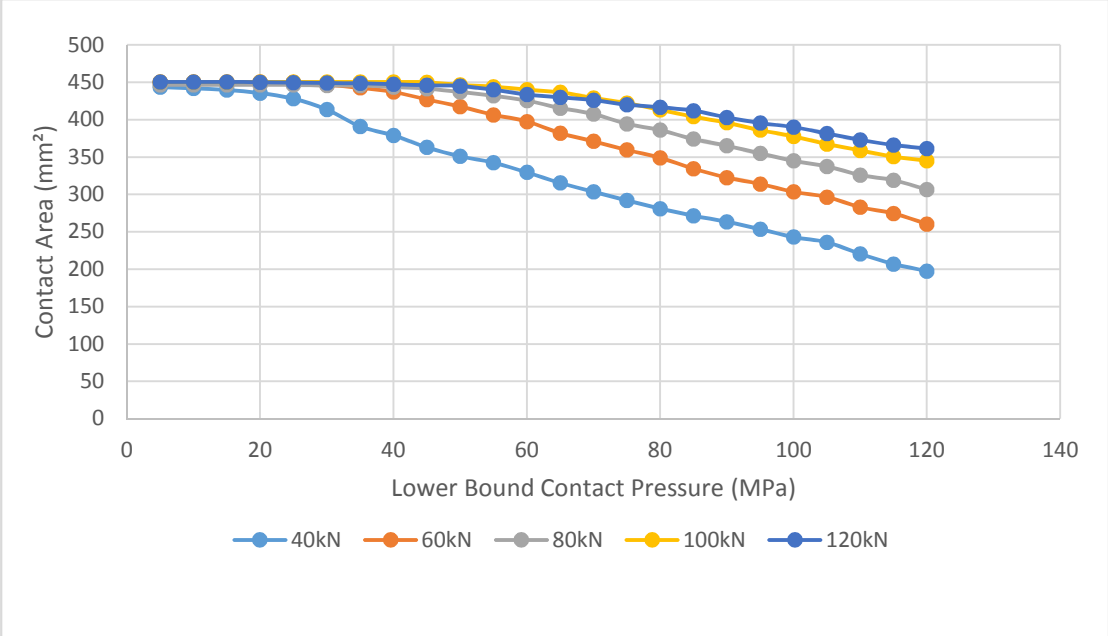

Figure 14. The contact area-lower bound pressure curve under different loads

Contact area for rolling speed of 5mm/s can be calculated in the same way. As shown in Figure 15, the contact areas and maximum contact pressures under all loads are compared with each other, data from forward tests are used.

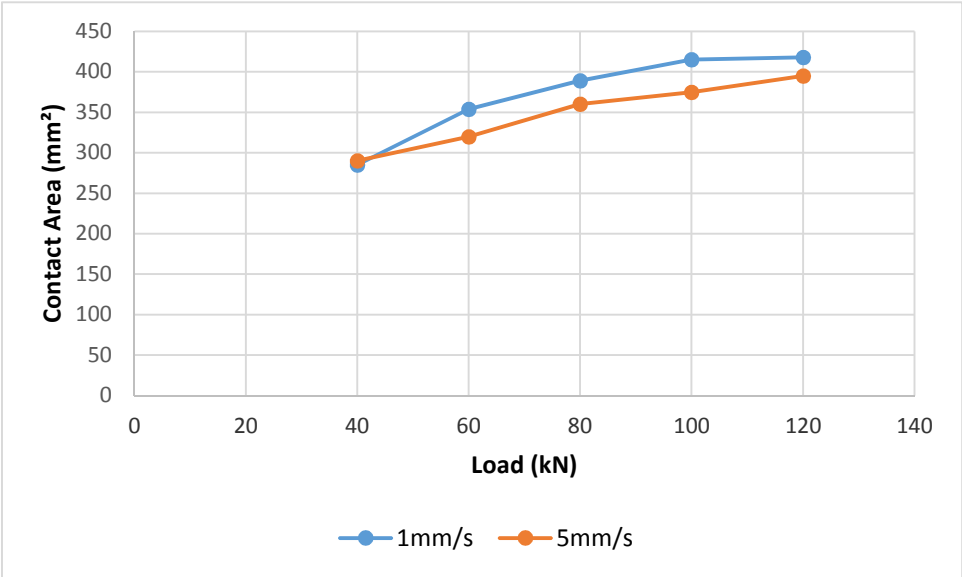

(a)

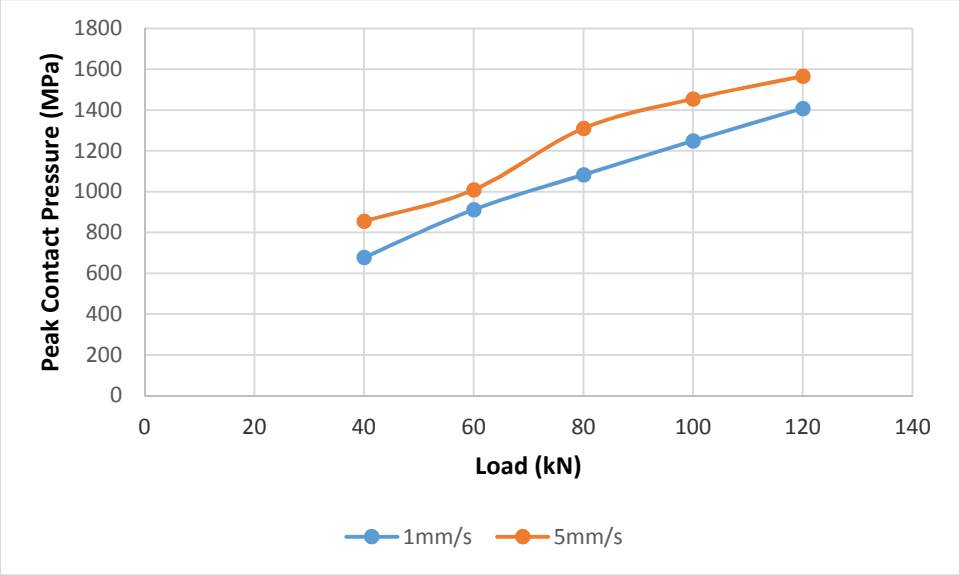

(b)

Figure 15. (a) Contact area comparison; (b) Maximum contact pressure comparison

The current software limits the highest measureable rolling speed at 5mm/s. By reconfiguring the software timing, it should be possible to measure rolling speeds of 100mm/s and faster.

3 Finite Element Analysis

3.1 Modelling Approach

To enable validation of the ultrasonic measurements, a three-dimensional finite element model of the contact patch between the wheel and the rail in the test rig was built using the commercial software Abaqus.

One whole wheel with a profile measured in the test rig for the ultrasonic measurements was modelled and a 1.6 m part of the rail with a standard UIC60 E1 profile (the rail profile in the rig has not been measured). The wheel radius was 0.46 m. The two profiles are shown in Figure 16 with their initial lateral positions. There is no inclination of the rail. Also, no angle of attack of the wheel is modelled. Details about the model are given in [16]. Since the shape and position are very sensitive to small deflections of the wheel and rail their whole geometry was modelled. In the contact region the mesh was refined (characteristic element length was less than 1.5mm). A convergence study was conducted. For both wheel and rail, elastic steel properties are used with a Young's modulus of 210 GPa and a Poisson's ratio of 0.3, respectively. To extend the work in the future, especially to study contact evolution with time, an elastic/platic approach could be used to take account of work hardening behaviour in the contact. The aim here though was a quick comparison, so the extra complexity was omitted. The vertical loads were chosen according to the ultrasonic measurements (40 kN to 120 kN in 20 kN steps). For the lateral loads (not applied in the measurements, but necessary in the model for defining a certain lateral position) a value of 5 kN is chosen. Friction coefficient was set to 0.5 which is a typical value of a dry wheel/rail contact.

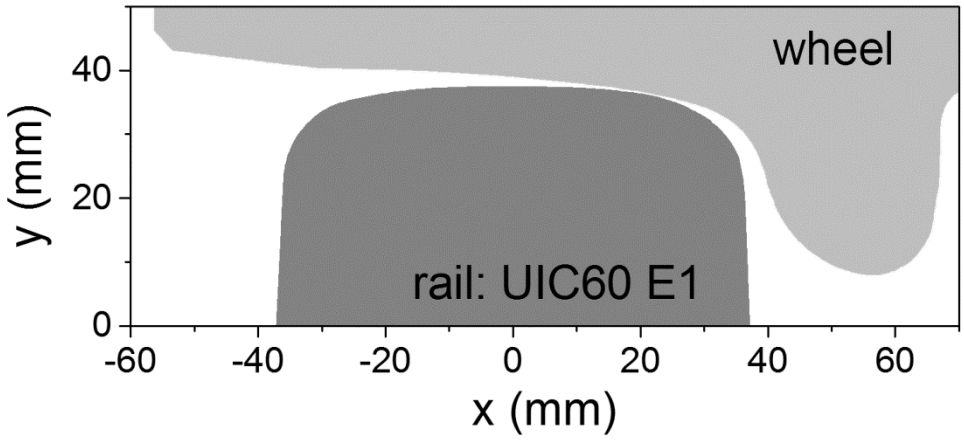

Figure 16: The measured wheel profile and the assumed rail profile used in the finite element model

The rail was modelled with and without the slot that contains the ultrasonic transducer. This slot is worked into the lower part rail head, as illustrated and dimensioned in Figure 17.

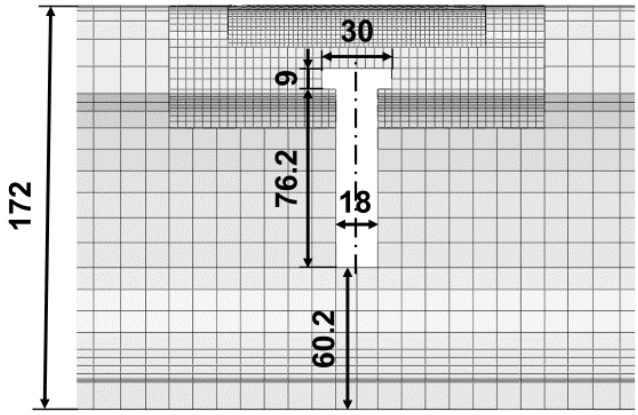

Figure 17: The slot worked into the rail with the corresponding dimensions in mm.

The main influence of the slot is due to the changed stiffness and bending stiffness of the rail in the region of the slot. For high lateral loads it is thus possible that the slot considerably changes the contact pressure distribution compared to a full rail. The vertical and lateral displacements for the two cases are shown in Figure 18. The maximum displacements in the rail with the slot are higher than in the rail without a slot due to the mentioned change in the bending stiffness. The difference, however, is only small and does not change the contact pressure distribution.

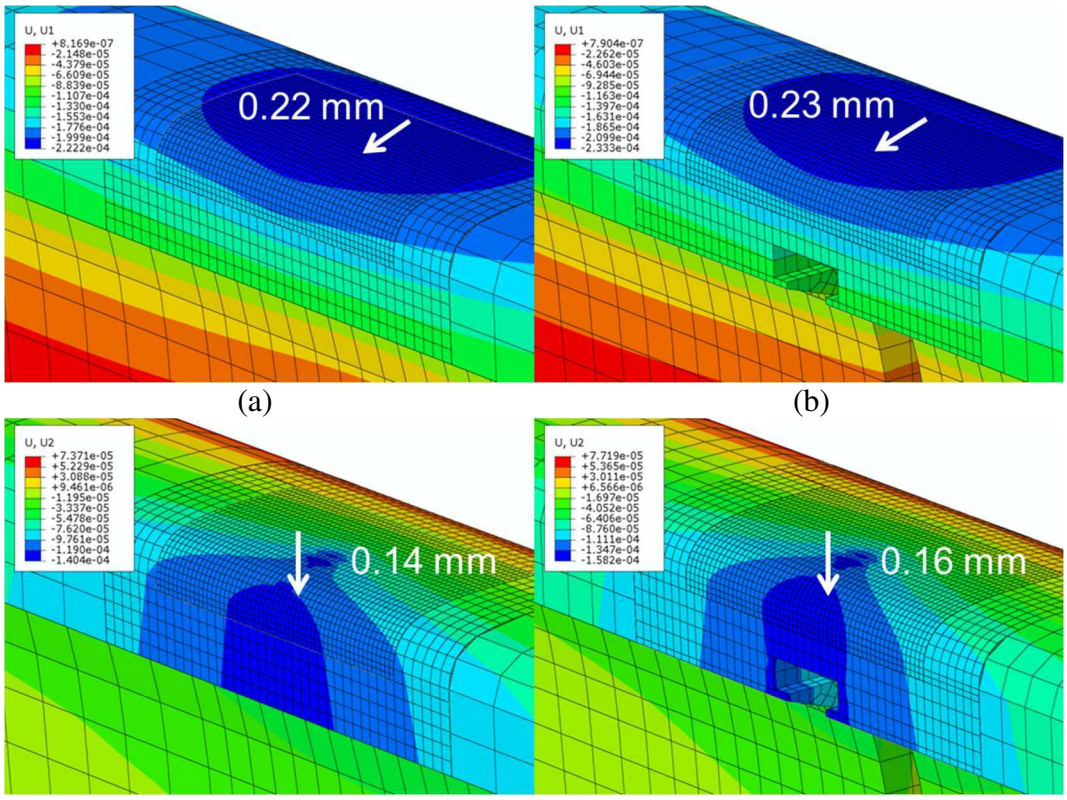

Figure 18: Lateral displacements in the rail for a) the model without a slot and b) the model with a slot and vertical displacements for c) the model without a slot and d) the model with a slot. The results correspond to the model with a vertical load of 120 kN

3.2 FE Results

Figure 19 shows contact pressure results for the highest load (120 kN vertical and 5 kN lateral load) in the model without and with a cavity worked into the rail. The pressure is evaluated when the wheel is situated directly above the slot. The maximum contact pressures are indicated for the two cases and are with 1445 MPa and 1442 MPa very similar. Also the contact pressure distribution is very similar in the two models. It can be assumed that for lower vertical loads the difference is even smaller.

Comparing the peak pressure result in Figure 19 with the peak pressure of 120 kN load from ultrasound measurements, it can be seen that the results are very close to each other. Multiple contact patches are also observed in FE results. The wheel and rail profiles used for FE analysis are new ones compared to worn wheel and rail in ultrasound tests, which is why there are some differences in contact shapes.

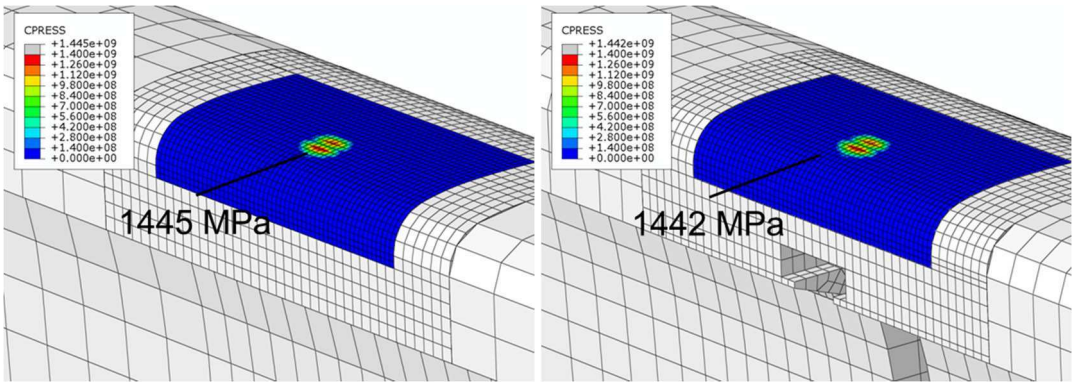

(a) (b)

Figure 19: Contact pressures for 120 kN vertical load for the a) the model without slot b) the model with a slot.

A picture of the tested wheel and rail was taken to show the approximate contact position as shown in Figure 20. From the picture it can be clearly seen that the contact position is located in the wheel tread-rail head contact zone. The white line (within the highlighted box) marks the contact "trace" as the wheel rolls over the rail, which gives a reasonable guide to where the contact is.

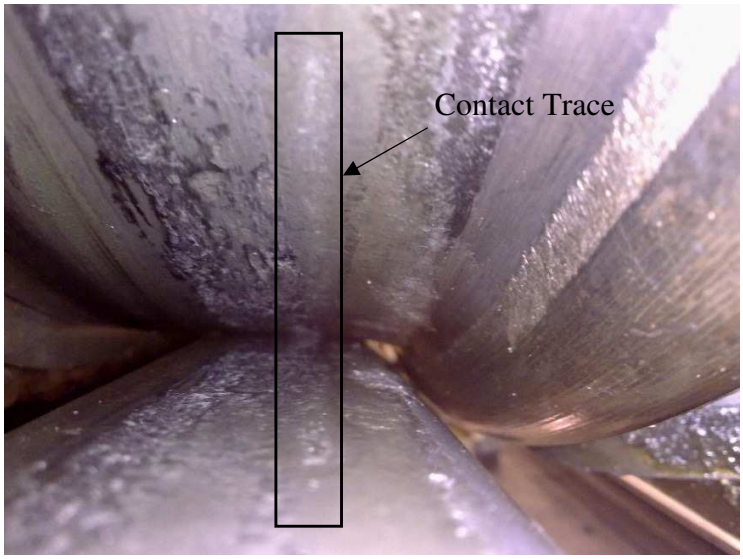

Figure 20: Actual wheel/rail contact

One contact pressure result was plotted on a 200mm long 3D UIC60A model according to position of the array (Figure 21). Compared with the real picture (Figure 20), position of the main contact looks roughly the same.

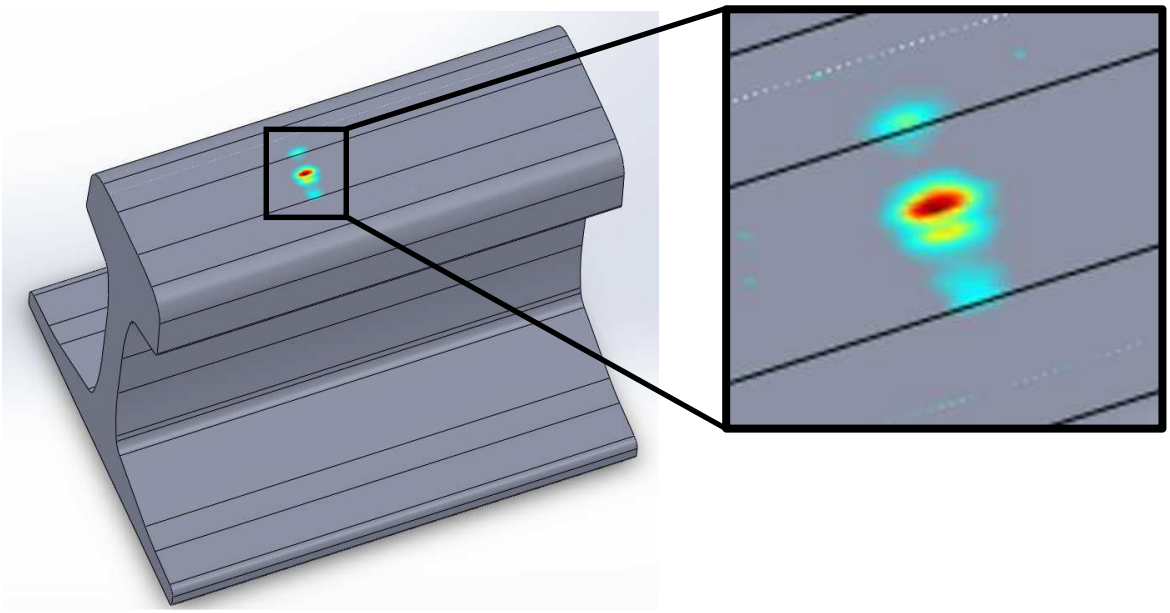

Figure 21: Contact pressure displayed on a 1:1 3D rail model

4 Conclusions

A method has been developed to characterise rolling contacts using a bespoke low cost ultrasonic array system. This was successfully applied to a simple rolling ball on flat arrangement. A rail mounted sensor was trialled in a static measurement and the results were positive with minimal displacement of the rail head due to the hole.

A full size wheel/rail rig was used to create a loaded wheel/rail interface for inspection. A rail mounted ultrasonic sensor was successfully used to measure the dynamic contact patch evolution. It is also possible to measure the contact pressure distribution with the aid of a calibration procedure. The current system is too slow for full speed rail, but with a commercial phased array system, the measurements would be possible at full speed.

Finite element analysis were carried out, dynamic wheel-rail contacts were simulated and contact patch and pressure distribution were obtained. The influence of a hole cut in the rail has been analysed.

The new ultrasonic measuring technique has been tested to successfully characterise dynamic contact and take real-time measurements using an ultrasonic scanning array. No significant difference were seen between forward and backward measurements under same load, which proves the stability of this method. Obvious changes in contact area and contact pressure were observed with increasing loads. With the current measuring equipment the effect of speed change on measurement has been characterised, however results from two speeds both display contact information clearly, which proves the capability of the technique at relative higher speeds.

According to FE simulations, the influence of a hole cut in the rail is very limited to the contact pressure results and the vertical deformation under loads. The peak pressure from FE simulations and ultrasound measurements matches with each other

well, which indicates the ultrasonic technique can be used as a good contact characterising and validating method other than FE analysis.

5 Proposed Future Work

Currently due to the limitation of the channel switching speed, the technique can only provide sufficient contact information of wheel-rail contacts at relative low speeds (wheel rolling speeds no higher than 50mm/s). In future work, with software and hardware upgraded, this technique can be capable of much higher speed. What is more important, more new arrays and mounting ways of the array will be developed to avoid channel switching, and eventually the ultrasound reflectometry technique is able to real-time characterise dynamic wheel-rail contact in actual field railway systems [17]. To apply this method to measure on the rail network, the ultrasonic pulsing hardware would have to be faster. By using a phased array ultrasonic system, it would be possible to increase measurement speed and resolution, but it would dramatically increase the associated costs and complications in post processing. Figure 22 shows the possible number of measurements as the wheel rolls over the rail at various speeds and various pulse repetition frequencies (PRF).

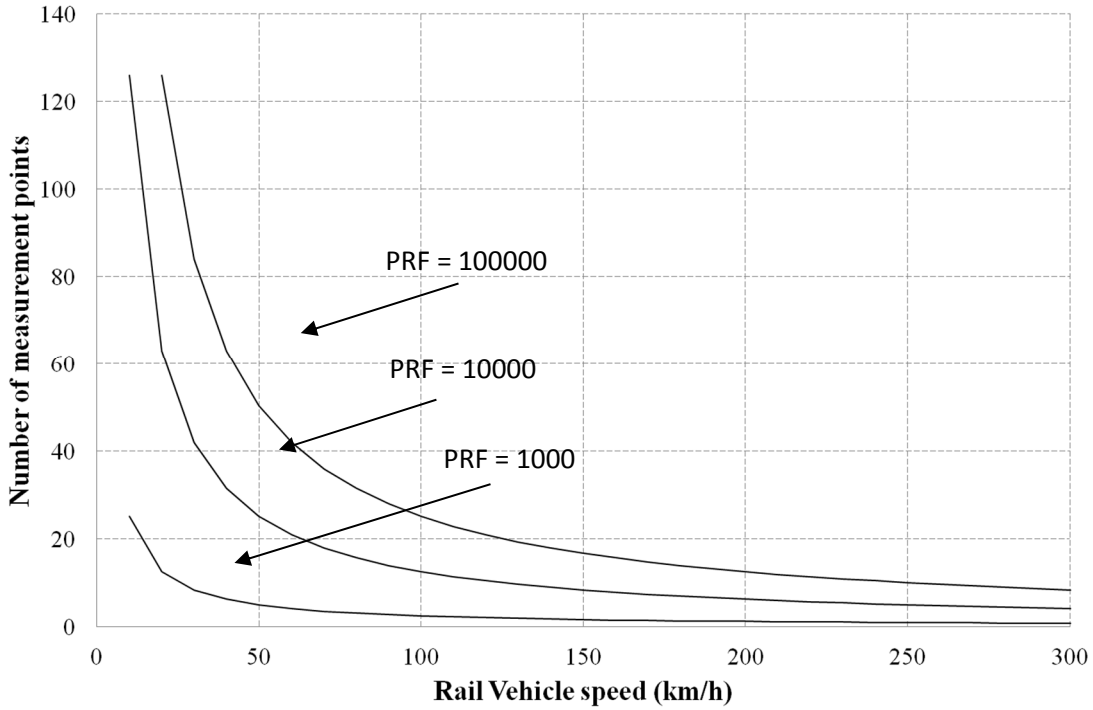

Figure 22. A graph showing the number of measuremens as the rail vehicle passes over the array transducer as a function of pulse repatition frequency.

Cutting a hole in the rail section is not an ideal solution and would not be permitted in a live rail network. It would be possible to mount the sensors at an angle on the outside of the rail head in pitch-catch configuration and achieve a similar result, although with lower resolution. It would also be possible to mount a series of sensors on the wheel but this would require the use of slip-rings or radio transmission.

Contact conditions are more severe during curving as the wheel/rail geometry becomes less conformal and contact occurs at the wheel flange. These conditions result in increased slip and resultant wear due to deformation and rolling contact fatigue [18]. Too much lateral load will result in excessive flange contact and wheel climb that can lead to derailment. So investigation of flange contacts is of greater importance than normal contacts.

By monitoring the position of the wheel on the rail during railroad vehicle movement, it would be possible to optimise speed with a safety feedback loop system thus preventing too much flange contact. By mounting sensors on the outside of the wheel, it would be possible to create a flange contact detection monitoring system. The transducers would have to be positioned in such a way that the signals could be reflected off the interface at precise locations. To do so might require some removal of wheel material or the use of a wedge to get the correct angle of attack as shown in Figure 23. A more in depth feasibility study can be seen in [19].

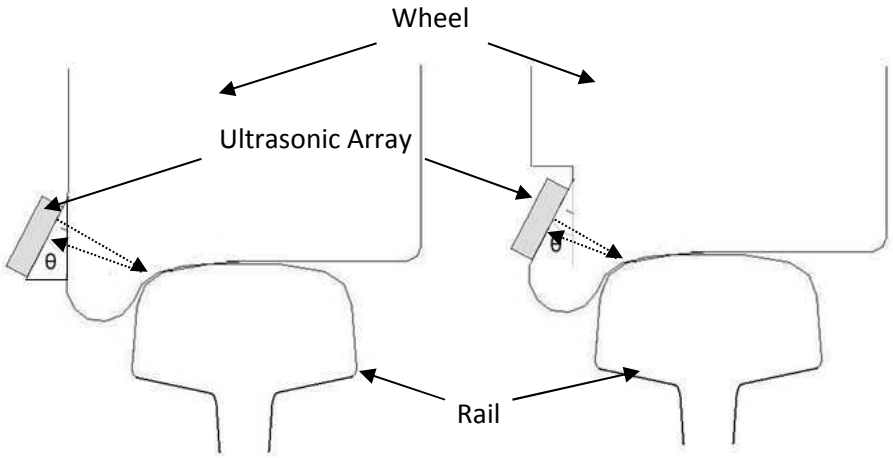

Figure 23. A diagram showing the possible options for transducer placement on the wheel for flange detection.

References

[1] W. Poole, 1987, "The Measurement of Contact Area between Opaque Objects under Static and Dynamic Rolling Conditions", *Proceedings of Contact Mechanics and Wear of the Wheel/rail System*, University of Rhode Island, Waterlooville Press, pp. 59-72.

[2] M. Pau, F. Aymerich, F. Ginesu, 2001, "Measurements of Nominal Contact Area in Metallic Surfaces: A Comparison between an Ultrasonic Method and a Pressure Sensitive Film", *Wear*, Vol. 249, pp. 533-535.

[3] I. Sebesan, Y. Zakaria, 2014, "Determination of Wheel-Rail Contact Characteristics by Creating a Special Program for Calculation", *Mathematical Modelling in Civil Engineering*, Vol. 10, No. 3, pp. 48-59.

[4] O. Polach, 2005, "Creep Forces in Simulations of Traction Vehicles Running on Adhesion Limit", *Wear*, Vol. 258, pp. 992-1000.

[5] J.J. Kalker, 1990, "Three-Dimensional Elastic Bodies in Rolling Contact", Kluwer Academic Publishers, Dordrecht/Boston/London, 314 pages.

[6] J.J. Kalker, 1982, "A Fast Algorithm for the Simplified Theory of Rolling Contact", *Vehicle System Dynamics*, Vol. 11, pp. 1-13.

[7] K.D. Vo, A.K. Tieu, H.T. Zhu, P.B. Kosasih, 2014, "A Tool to Estimate the Wheel/Rail Contact and Temperature Rising under Dry, Wet and Oily Conditions", *COMPRAIL 14th Conference on Railway Engineering Design and Optimization*, Vol. 135, pp. 191-201.

[8] Z. Li, X. Zhao, C. Esveld, R.P.B.J. Dollevoet, 2007, "The Dynamic Stress State of the Wheel–Rail Contact", in *Proceedings of IASME/WSEAS International Conference on Continuum Mechanics*, 15th-17th May 2007, Portorose, Slovenia, pp. 127-133.

[9] R.S. Dwyer-Joyce, B.W. Drinkwater, 2003, "In-situ Measurement of Contact Area and Pressure Distribution in Machine Elements", *Tribology Letters*, Vol. 14, pp. 41-52.

[10] M.B. Marshall, R. Lewis, R.S. Dwyer-Joyce, U. Olofsson, S. Björklund, 2006, "Experimental Characterisation of Wheel-Rail Contact Patch Evolution", *ASME Journal of Tribology*, Vol. 128, pp. 493-504.

[11] R.S. Dwyer-Joyce, C. Yao, J. Zhang, R. Lewis, B.W. Drinkwater, 2009, "Feasibility Study for Real Time Measurement of Wheel/Rail Contact using an Ultrasonic Array", *ASME Journal of Tribology*, Vol. 131, No. 4, Paper TRIB-08-1189.

[12] M. Pau, F. Aymerich, F. Ginesu, 2002, "Distribution of Contact Pressure in Wheel–Rail Contact Area", *Wear*, Vol. 253, pp. 265-274.

[13] R.S. Dwyer-Joyce, B.W. Drinkwater, A. Quinn, 2001, "The Use of Ultrasound in the Investigation of Rough Surface Interfaces", *ASME Journal of Tribology*, Vol. 123, pp. 8-16.

[14] H. Brunskill, L. Zhou, R. Lewis, 2016, "Feasibility of using Ultrasound for Real Time Dynamic Characterisation of the Wheel/Rail Contact", submitted to *Proceedings of the Institution of Mechanical Engineers, Part J, Journal of Engineering Tribology*.

[15] J. McEwen, R. F. Harvey, 1987, "Full-Scale Wheel-on-Rail Wear Testing: Comparisons with Service Wear and a Developing Theoretical Predictive Method", *Lubrication Engineering*, Vol. 41, No. 2, pp. 80-88.

[16] M. Pletz, W. Daves, W. Yao, W. Kubin, S. Scheriau, 2014, "Multi-Scale Finite Element Modelling to Describe Rolling Contact Fatigue in a Wheel–Rail Test Rig", *Tribology International*, Vol. 80, pp. 147-55.

[17] L. Zhou, H. Brunskill, R. Lewis, "Real-Time Non-Invasive Measurement and Monitoring of Wheel–Rail Contact using Ultrasonic Reflectometry", submitted to *Structural Health Monitoring.*

[18] D.F. Cannon, H. Pradier, 1996, "Rail Rolling Contact Fatigue – Research by the European Rail Research Institute", *Wear*, Vol. 191, pp. l-13.

[19] R.S. Dwyer-Joyce, C. Yao, R. Lewis, H. Brunskill, 2012, "An Ultrasonic Sensor for Monitoring Wheel Flange/Rail Gauge Corner Contact". *Proceedings of the Institution of Mechanical Engineers, Part F, Journal of Rail and Rapid Transit,* Vol. 227, No. 2, pp. 188-195.